

SMAFormer: Synergistic Multi-Attention Transformer for Medical Image Segmentation

Fuchen Zheng¹², Xuhang Chen¹²³, Weihuang Liu¹, Haolun Li¹,
Yingtie Lei¹, Jiahui He²⁴, Chi-Man Pun^{1*}, and Shoujun Zhou^{2*}

¹University of Macau

²Shenzhen Institutes of Advanced Technology, Chinese Academy of Sciences

³Huizhou University

⁴University of Nottingham Ningbo China

Abstract—In medical image segmentation, specialized computer vision techniques, notably transformers grounded in attention mechanisms and residual networks employing skip connections, have been instrumental in advancing performance. Nonetheless, previous models often falter when segmenting small, irregularly shaped tumors. To this end, we introduce SMAFormer, an efficient, Transformer-based architecture that fuses multiple attention mechanisms for enhanced segmentation of small tumors and organs. SMAFormer can capture both local and global features for medical image segmentation. The architecture comprises two pivotal components. First, a Synergistic Multi-Attention (SMA) Transformer block is proposed, which has the benefits of Pixel Attention, Channel Attention, and Spatial Attention for feature enrichment. Second, addressing the challenge of information loss incurred during attention mechanism transitions and feature fusion, we design a Feature Fusion Modulator. This module bolsters the integration between the channel and spatial attention by mitigating reshaping-induced information attrition. To evaluate our method, we conduct extensive experiments on various medical image segmentation tasks, including multi-organ, liver tumor, and bladder tumor segmentation, achieving state-of-the-art results. Code and models are available at: <https://github.com/lzeeorno/SMAFormer>.

Index Terms—Transformer, Tumor Segmentation, Medical Image Segmentation, Feature Fusion, Attention Mechanism

I. INTRODUCTION

Early tumor diagnosis is crucial as late-stage cancer is often incurable [1]. Artificial intelligence, particularly medical image segmentation, plays a vital role in this early diagnosis [2]–[5]. However, accurately segmenting medical images, especially tiny tumors or organs, remains challenging due to feature loss in deep convolutional networks.

While recent Convolutional Neural Network (CNN) based methods [6]–[13] show promise, their ability to capture small object features is limited. Multi-attention mechanisms [14]–[22] offer some improvement but still lack optimal integration and performance.

This paper introduces **SMAFormer**, an efficient and effective Transformer-based model for medical image segmentation. Inspired by ResUNet [23], SMAFormer combines Transformer blocks with a U-shaped residual structure for enhanced multi-resolution feature learning.

Our key contributions are:

- 1) **SMAFormer Architecture**: A novel residual U-shaped Transformer model integrating attention mechanisms, U-shaped architecture, and residual connections for efficient and effective medical image segmentation.
- 2) **Learnable Segmentation Modulator**: An embeddable module for multi-scale feature fusion, enhancing the synergy between different attention mechanisms.
- 3) **State-of-the-art Performance**: Extensive experiments demonstrate SMAFormer achieves state-of-the-art results on various medical image segmentation datasets.

II. RELATED WORK

A. Medical Image Segmentation

Medical image segmentation involves partitioning medical images into distinct regions. The U-Net architecture [24] is widely recognized for its ability to extract detailed features while maintaining contextual information, leading to several derivatives like ResUNet [23], which combines U-Net with ResNet [25]. ResNet’s residual connections, which help prevent vanishing gradients by ensuring smooth information flow, significantly boost segmentation performance. Our SMAFormer integrates skip and residual connections to optimize segmentation outcomes.

B. Vision Transformer

Transformers, with their global self-attention mechanisms, excel at capturing long-range dependencies in images, as demonstrated by Vision Transformer (ViT) [26]. This architecture outperforms traditional CNNs in image classification and has been adapted for medical imaging, with models like the Swin Transformer [27] gaining popularity. Hybrid models like ResT [28] combine ResNet and transformers for enhanced performance.

In medical image segmentation, attention mechanisms have been integrated into U-Net architectures, giving rise to U-shaped transformers like TransUNet [29], which combines CNNs and transformers to encode global context. However, many existing models, including TransUNet [29], do not fully exploit the transformer’s potential. To address this, we propose a residual U-shaped Transformer-based structure that

* Corresponding Authors.

effectively fuses attention mechanisms, aiming to improve segmentation performance.

III. METHOD

A. Overview

SMAFormer, as depicted in Figure 1, adopts a hierarchical U-shaped architecture reminiscent of ResU-Net [30], [31], incorporating skip-connections and residual connections between the encoder and decoder for efficient information propagation.

Given a 3D medical image $I \in \mathbb{R}^{3 \times H \times W}$, SMAFormer first extracts low-level features through an initial projection layer comprising a 3×3 convolution followed by a ReLU activation. The extracted features are then passed through a four-stage encoder, mirroring the U-Net structure. Each encoder stage consists of a stack of SMA Transformer blocks (detailed in Section III-B) for capturing multi-scale features, followed by a down-sampling layer.

The down-sampling layer performs two crucial operations. First, it records positional information within the embedded modulator (discussed in Section III-C). Second, it utilizes a residual convolution block which consist by three 3×3 convolutions with a stride of 2 to reduce the spatial dimensions of the feature maps while increasing the channel count. This down-sampling process is enriched by residual connections, enabling the preservation of long-range dependencies. Specifically, given an input feature map $X_i \in \mathbb{R}^{C \times H \times W}$, the output of the i -th encoder stage is $X_{\text{conv}} + X_{\text{residual}} \in \mathbb{R}^{2^i C \times \frac{H}{2^i} \times \frac{W}{2^i}}$, where X_{conv} denotes the convolved features and X_{residual} represents the features from the residual connection.

Mirroring the encoder, the decoder comprises four symmetrical stages. Each stage begins with a 2×2 transposed convolution to upsample the feature maps, effectively halving the channel count and doubling the spatial dimensions. Subsequently, the upsampled features are concatenated with the corresponding encoder features via skip connections, facilitating the fusion of high-level semantic information with low-level spatial details. Finally, an output convolution layer processes the concatenated features to generate the segmentation prediction.

B. SMA Block

Directly applying conventional Transformers [32] to medical image segmentation presents two significant challenges: (1) **Difficulty in Assigning Attention to Relevant Regions**: Transformers, especially when not fine-tuned for medical images, often struggle to focus attention on medically relevant regions, hindering their performance in multi-organ or multi-tumor segmentation tasks. (2) **Limited Capture of Local Context**: Local context plays a crucial role in accurately segmenting small structures like organs or tumors. Traditional Transformers, with their global receptive fields, often fail to adequately capture this local information.

To address these challenges, we introduce the Synergistic Multi-Attention (SMA) Transformer block, illustrated in Figure 1. This block leverages the combined strengths of three

distinct attention mechanisms and multi-head self-attention to achieve robust and accurate segmentation.

1) *Synergistic Multi-Attention (SMA)*: Unlike approaches that restrict self-attention within local windows [31], SMA employs a combination of channel attention, spatial attention, and pixel attention in conjunction with multi-head self-attention. This synergistic approach enables the model to effectively capture multi-scale features and handle potential deformations within the medical images as depicted in Figure 1 (b). Given a feature map $X \in \mathbb{R}^{C \times H \times W}$, SMA first divides it into patches and flattens the channels. The flattened features are then processed by the three attention mechanisms (channel attention, pixel attention, and spatial attention) in parallel. The outputs from the pixel and channel attention branches are combined through matrix multiplication and further processed by the spatial attention branch. Finally, the outputs from all three branches are fused to generate the final attention map.

2) *Enhanced Multi-Layer Perceptron (E-MLP)*: Recognizing the limitations of standard Feed-Forward Networks (FFNs) in capturing local context [33], [34], we enhance the E-MLP within our Transformer block by incorporating depth-wise and pixel-wise convolutions [35]–[37]. As depicted in Figure 1 (c), the E-MLP first projects the input tokens to a higher dimensional space using a linear layer. The projected tokens are then reshaped into 2D feature maps and processed by a 3×3 pixel-wise convolution followed by a 3×3 depth-wise convolution, effectively capturing local contextual information. The resulting features are then reshaped back into tokens and projected back to the original channel dimension using another linear layer. Finally, a GELU activation function [38] is applied to introduce non-linearity.

Mathematically, the computation within an SMA Transformer block can be expressed as:

$$\begin{aligned} X'_{i+1} &= \text{SMA}(\text{LN}(X_i)) + X_i, \\ X_{i+1} &= \text{E-MLP}(\text{LN}(X'_{i+1})) + X'_{i+1}, \end{aligned} \quad (1)$$

where X_i represents the input features to the i -th block, X'_{i+1} and X_{i+1} are the outputs of the SMA and E-MLP modules respectively, and LN denotes layer normalization.

The synergistic interplay between SMA and E-MLP within each SMA Transformer block enables SMAFormer to effectively capture both global and local contextual information, leading to improved segmentation performance.

C. Multi-Scale Segmentation Modulator

To further enhance SMAFormer's ability to capture fine-grained details and facilitate synergistic multi-attention, we introduce the multi-scale segmentation modulator as shown in Figure 2.

D. Objective Function

We train SMAFormer using the BCE Dice loss \mathcal{L}_{BD} [39], a widely adopted loss function for segmentation tasks that combines the benefits of Binary Cross-Entropy (BCE) loss \mathcal{L}_{BCE} and Dice loss \mathcal{L}_D :

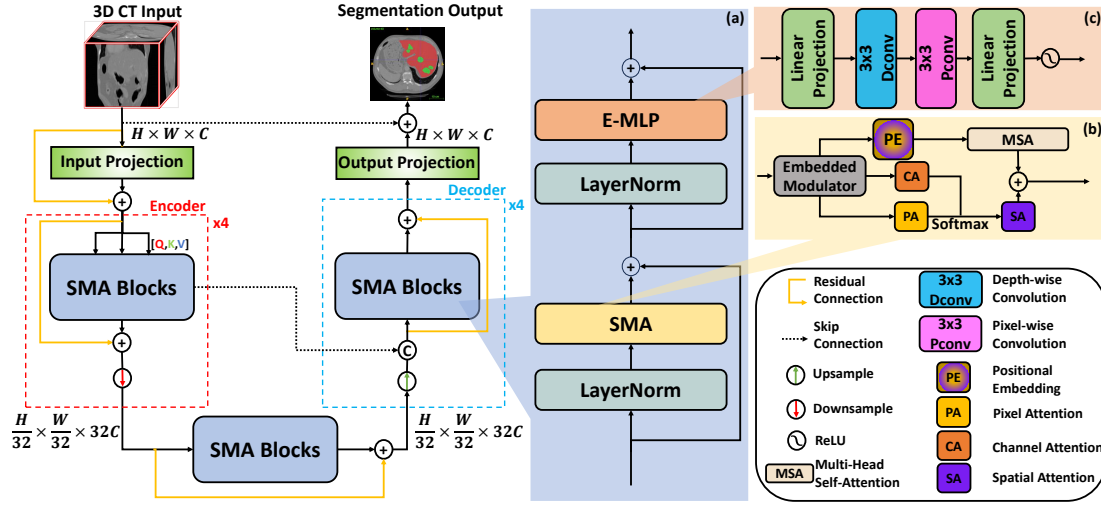


Fig. 1. This figure provides an overview of the SMAFormer architecture. The figure details (a) the SMA Transformer block, (b) the SMA Part within the SMA Transformer block, and (c) the E-MLP Part within the SMA Transformer block.

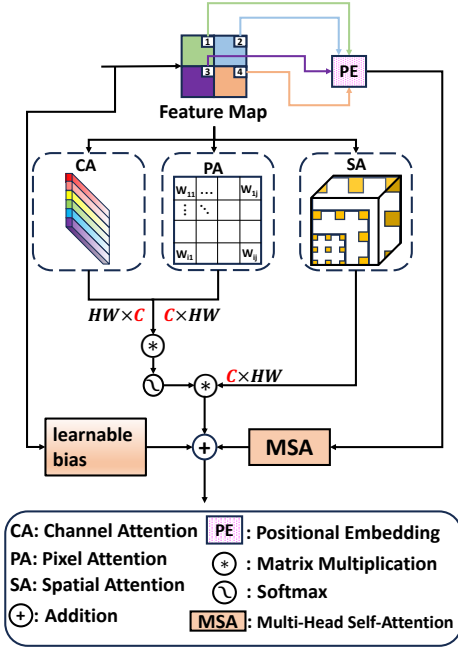


Fig. 2. This figure presents a schematic diagram of the proposed modulator.

$$\begin{aligned} \mathcal{L}_{BD} &= \mathcal{L}_D + \mathcal{L}_{BCE}(y, p) \\ &= \frac{1}{N} \sum_{i=1}^N \left(1 - \frac{2 \sum_j y_{i,j} p_{i,j}}{\sum_j y_{i,j} + \sum_j p_{i,j}} \right) \\ &\quad - (y \log(p) + (1 - y) \log(1 - p)), \end{aligned} \quad (2)$$

where y represents the ground truth segmentation mask, p denotes the predicted segmentation mask, and N is the number of pixels in the image. The BCE loss penalizes discrepancies between the predicted and true label distributions, while the Dice loss encourages overlap between the predicted and true segmentation regions. This combined loss function encourages

both accurate pixel-wise classification and strong boundary delineation.

IV. EXPERIMENTS

A. Datasets and Implementation Details

This work utilizes three publicly available medical image segmentation datasets: LiTS2017 [44], ISICDM2019 [45], and Synapse [46]. Following nnformer [43], we employ an 80/15/5 train/validation/test split for all datasets. Input images are resized to 512×512 pixels.

SMAFormer is implemented in PyTorch and trained on a single NVIDIA GeForce RTX 4090 GPU using SGD with momentum (0.98), weight decay ($1e^{-6}$), and a cosine-decayed learning rate (initial: $1e^{-2}$, minimum: $6e^{-6}$). Data augmentation includes random horizontal flipping and rotation. We utilize a pre-trained model from ViT [47].

B. Evaluation Metrics

We evaluated the segmentation performance using two widely adopted metrics: **Dice Coefficient Score (DSC)** and **Mean Intersection over Union (mIoU)**.

$$DSC = \frac{2 \times |P \cap G|}{|P| + |G|}, \quad (3)$$

where P represents the predicted segmentation. G represents the ground truth segmentation. $|P \cap G|$ represents the number of pixels in the intersection of the predicted and ground truth segmentations. $|P|$ represents the number of pixels in the predicted segmentation. $|G|$ represents the number of pixels in the ground truth segmentation.

$$mIoU = \frac{1}{C} \sum_{i=1}^C \frac{|P_i \cap G_i|}{|P_i| + |G_i| - |P_i \cap G_i|}, \quad (4)$$

where C represents the number of classes. P_i represents the predicted segmentation for class i . G_i represents the ground truth segmentation for class i .

TABLE I
COMPARISON WITH STATE-OF-THE-ART MODELS ON THE ISICDM2019 AND LITS2017 DATASETS. THE BEST RESULTS ARE BOLDIED WHILE THE SECOND BEST ARE UNDERLINED.

Method	ISIDM2019				LITS2017			
	Average		Bladder	Tumor	Average		Liver	Tumor
	DSC(%) ↑	mIoU(%) ↑	DSC(%) ↑	DSC(%) ↑	DSC(%) ↑	mIoU(%) ↑	DSC(%) ↑	DSC(%) ↑
ViT [26]+CUP [29]	88.60	84.40	91.88	85.32	80.33	77.25	83.97	76.69
R50-ViT [26]+CUP [29]	88.77	85.62	92.05	85.49	82.62	79.68	85.83	79.41
ResUNet++ [30]	87.11	83.78	89.90	84.32	75.73	74.19	79.12	72.34
ResT-V2-B [28]	89.26	82.13	93.01	85.50	78.53	75.24	81.22	75.83
TransUNet [29]	<u>94.56</u>	<u>93.60</u>	<u>97.74</u>	<u>91.38</u>	<u>93.28</u>	<u>90.81</u>	<u>95.54</u>	<u>91.03</u>
SwinUNet [40]	91.95	89.77	94.73	89.17	89.68	86.62	93.31	86.04
Swin UNETR [41]	92.60	90.61	95.08	90.12	91.95	90.02	94.73	89.17
UNETR [42]	91.55	88.34	94.83	88.26	89.38	87.46	92.89	85.86
nnFormer [43]	93.54	89.11	96.97	90.41	91.74	89.95	94.57	88.91
SMAFormer(Ours)	96.07	94.67	98.57	93.56	94.11	91.94	95.88	92.34

TABLE II
COMPARISON WITH STATE-OF-THE-ART MODELS ON THE SYNAPSE MULTI-ORGAN DATASET. THE BEST RESULTS ARE BOLDIED WHILE THE SECOND BEST ARE UNDERLINED.

Model	Average DSC(%)↑	Aorta DSC(%)↑	Gallbladder DSC(%)↑	Kidney(Left) DSC(%)↑	Kidney(Right) DSC(%)↑	Liver DSC(%)↑	Pancreas DSC(%)↑	Spleen DSC(%)↑	Stomach DSC(%)↑
ViT [26]+CUP [29]	67.86	70.19	45.10	74.70	67.40	91.32	42.00	81.75	70.44
R50-ViT [26]+CUP [29]	71.29	73.73	55.13	75.80	72.20	91.51	45.99	81.99	73.95
TransUNet [29]	84.36	90.68	<u>71.99</u>	86.04	83.71	95.54	73.96	88.80	84.20
SwinUNet [40]	79.13	85.47	66.53	83.28	79.61	94.29	56.58	<u>90.66</u>	76.60
UNETR [42]	79.56	89.99	60.56	85.66	84.80	94.46	59.25	87.81	73.99
Swin UNETR [41]	73.51	82.94	60.96	80.41	71.14	91.55	56.71	77.46	66.94
CoTr [48]	<u>85.72</u>	92.96	71.09	85.70	85.71	<u>96.88</u>	81.28	90.44	81.74
nnFormer [43]	85.32	90.72	71.67	85.60	<u>87.02</u>	<u>96.28</u>	82.28	87.30	81.69
SMAFormer(Ours)	86.08	<u>92.13</u>	72.03	86.97	88.60	97.71	<u>81.93</u>	91.77	<u>84.15</u>

C. Comparisons with State-of-the-Art Methods

This subsection compares SMAFormer’s performance with state-of-the-art methods (Tables I and II).

1) *Liver Tumor Segmentation (Table I)*: SMAFormer achieves superior performance (DSC: 94.11%, mIoU: 91.94%), surpassing all compared methods including TransUNet (DSC: 93.28%, mIoU: 90.81%). This highlights its effectiveness in segmenting small, irregular tumors, attributed to the synergistic multi-attention mechanism and feature fusion modulator.

2) *Bladder Tumor Segmentation (Table I)*: SMAFormer again demonstrates superior performance (DSC: 96.07%, mIoU: 94.67%). Notably, it improves the Dice coefficient by 2.18% on average for tumor segmentation compared to the second-best model. This showcases its ability to accurately delineate tumor boundaries, even in challenging cases, attributed to the E-MLP within the SMA Transformer block.

3) *Multi-Organ Segmentation (Table II)*: SMAFormer achieves state-of-the-art results on the Synapse dataset (average DSC: 86.08%), with the highest DSC scores for five out of eight organs. While it slightly lags behind in a few metrics due to task complexity, its performance underscores its potential for multi-organ segmentation tasks.

D. Visualization of Segmentation Results

Figure 3 showcases SMAFormer’s superior performance on the LiTS2017 dataset, accurately segmenting small tumor nodules that other methods struggle with.

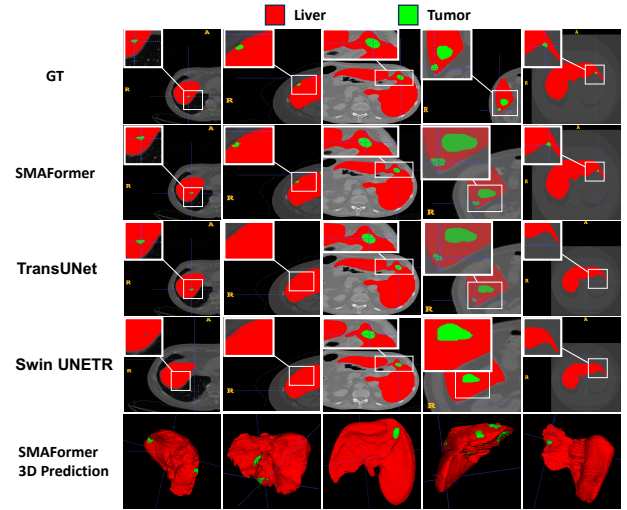


Fig. 3. LiTS2017 Prediction Result.

Figure 4 illustrates SMAFormer’s accurate segmentation on challenging ISICDM2019 cases, even with small tumors with irregular shapes.

Figure 5 demonstrates SMAFormer’s consistent and accurate segmentation across various abdominal organs in the Synapse dataset, highlighting its robustness and generalization ability.

In summary, SMAFormer consistently outperforms existing

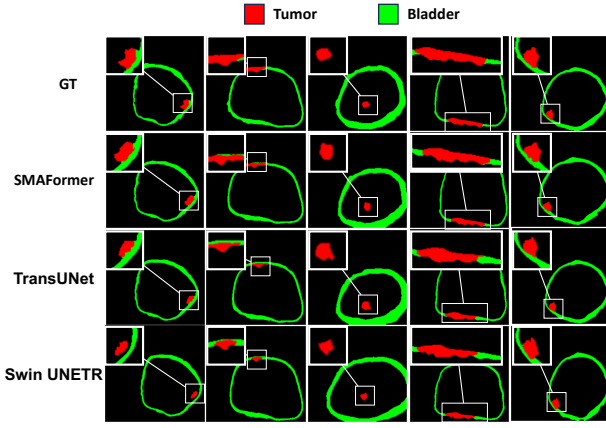


Fig. 4. ISICDM2019 Prediction Result.

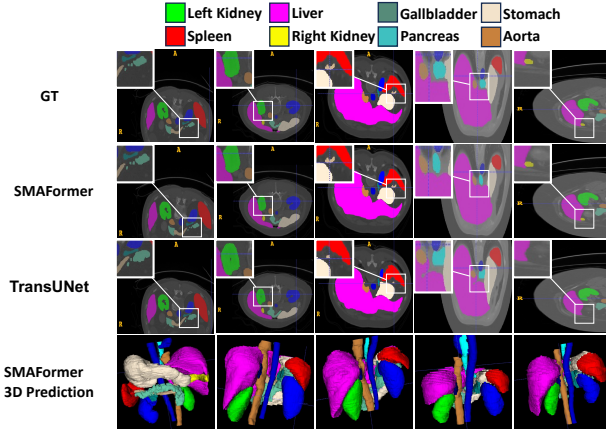


Fig. 5. Synapse Prediction Result.

methods across diverse medical image segmentation tasks. Its superior performance is attributed to the synergistic combination of the SMA Transformer block, feature fusion modulator, and E-MLP, demonstrating its potential as a powerful tool for medical image segmentation.

E. Ablation Study

This subsection examines the impact of each component within SMAFormer through an ablation study conducted on the ISICDM2019 and LiTS2017 datasets (experimental setup identical to Section IV-A). Table III summarizes the results.

TABLE III
ABLATION STUDY OF DIFFERENT MODULES IN SMAFORMER.

SMA	E-MLP	Modulator	ISICDM2019 Average DSC \uparrow	LiTS2017 Average DSC \uparrow
✓	✗	✗	82.28%	79.95%
✗	✓	✗	80.54%	75.67%
✗	✗	✓	78.41%	73.20%
✓	✓	✗	89.53%	88.47%
✓	✗	✓	86.31%	84.26%
✓	✓	✓	96.07%	94.61%

Replacing the SMA block with a standard Transformer block (multi-head self-attention only) decreased performance

across both datasets, highlighting the importance of integrating channel, spatial, and pixel attention for comprehensive feature representation in medical images (Table III).

Similarly, substituting the E-MLP module with a standard FFN led to reduced performance, emphasizing the value of depth-wise and pixel-wise convolutions within the E-MLP for capturing local context (Table III).

Removing the multi-scale segmentation modulator also degraded performance, confirming its role in facilitating synergistic multi-attention and enhancing fine-grained detail capture.

In conclusion, the ablation study demonstrates that the SMA block, E-MLP module, and multi-scale segmentation modulator are all essential for SMAFormer's superior performance in medical image segmentation.

V. CONCLUSION

In this paper, we presented SMAFormer, a novel Transformer-based architecture designed for efficient and accurate medical image segmentation. The key innovation lies in the Synergistic Multi-Attention block, which effectively integrates pixel, channel, and spatial attention mechanisms to capture both local and global contextual information. This synergistic approach addresses the limitations of conventional Transformers in accurately segmenting small and irregularly shaped tumors and organs commonly found in medical images. Furthermore, the introduction of a multi-scale segmentation modulator enhances SMAFormer's ability to preserve salient features across different scales and further facilitates the synergistic interplay between the multiple attention mechanisms. Extensive experiments conducted on three publicly available medical image segmentation datasets demonstrate that SMAFormer achieves state-of-the-art performance, surpassing existing methods in accurately segmenting various organs and tumors. The promising results obtained in this study highlight the potential of SMAFormer as a robust and effective tool for assisting medical professionals in diagnosis, treatment planning, and disease monitoring.

VI. ACKNOWLEDGMENT

This work was supported in part by the University of Macau under Grant MYRG2022-00190-FST, and in part by the Science and Technology Development Fund, Macau SAR, under Grant 0141/2023/RIA2 and 0193/2023/RIA3, in part by the Natural Science Foundation of Guangdong Province (No. 2023A1515010673), and in part by the Shenzhen Technology Innovation Commission (No. JSGG20220831110400001), and in part by Shenzhen Medical Research Fund (No. D2404001), and in part by Shenzhen Engineering Laboratory for Diagnosis & Treatment Key Technologies of Interventional Surgical Robots (XMHT20220104009), and The Key Laboratory of Biomedical Imaging Science and System, CAS, for the Research platform support.

REFERENCES

- [1] G. P. Dunn, A. T. Bruce, H. Ikeda, L. J. Old, and R. D. Schreiber, "Cancer immunoediting: from immunosurveillance to tumor escape," *Nature immunology*, vol. 3, no. 11, pp. 991–998, 2002.
- [2] T. Zhou, X. Chen, Y. Shen, M. Nieuwoudt, C.-M. Pun, and S. Wang, "Generative ai enables eeg data augmentation for alzheimer's disease detection via diffusion model," in *ISPC-ASIA*, 2023, pp. 1–6.
- [3] X. Chen, C.-M. Pun, and S. Wang, "Medprompt: Cross-modal prompting for multi-task medical image translation," *arXiv*, 2023.
- [4] X. Chen, B. Lei, C.-M. Pun, and S. Wang, "Brain diffuser: An end-to-end brain image to brain network pipeline," in *PRCV*, 2023, pp. 16–26.
- [5] C. Gong, C. Jing, X. Chen, C. M. Pun, G. Huang, A. Saha, M. Nieuwoudt, H.-X. Li, Y. Hu, and S. Wang, "Generative ai for brain image computing and brain network computing: a review," *Frontiers in Neuroscience*, vol. 17, p. 1203104, 2023.
- [6] X. Liu, G. Huang, X. Yuan, Z. Zheng, G. Zhong, X. Chen, and C.-M. Pun, "Weakly supervised semantic segmentation via saliency perception with uncertainty-guided noise suppression," *The Visual Computer*, pp. 1–16, 2024.
- [7] H. Li, G. Huang, X. Yuan, Z. Zheng, X. Chen, G. Zhong, and C.-M. Pun, "Psanet: prototype-guided salient attention for few-shot segmentation," *The Visual Computer*, pp. 1–15, 2024.
- [8] H. Tang, G. Huang, L. Cheng, X. Yuan, Q. Tao, X. Chen, G. Zhong, and X. Yang, "Rm-unet: Unet-like mamba with rotational ssm module for medical image segmentation," *Signal, Image and Video Processing*, 2024.
- [9] Y. Jiang, X. Chen, C.-M. Pun, S. Wang, and W. Feng, "Mfdnet: Multi-frequency deflare network for efficient nighttime flare removal," *The Visual Computer*, pp. 1–14, 2024.
- [10] W. Wu, T. Dai, X. Huang, F. Ma, and J. Xiao, "Image augmentation with controlled diffusion for weakly-supervised semantic segmentation," in *ICASSP*, 2024, pp. 6175–6179.
- [11] —, "Top-k pooling with patch contrastive learning for weakly-supervised semantic segmentation," *arXiv*, 2023.
- [12] W. Wu, T. Dai, Z. Chen, X. Huang, F. Ma, and J. Xiao, "Apc: Adaptive patch contrast for weakly supervised semantic segmentation," *arXiv*, 2024.
- [13] Q. Zhao, X. Zhang, H. Tang, C. Gu, and S. Zhu, "Enlighten-anything: When segment anything model meets low-light image enhancement," *arXiv*, 2023.
- [14] X. Chen, X. Cun, C.-M. Pun, and S. Wang, "Shadocnet: Learning spatial-aware tokens in transformer for document shadow removal," in *ICASSP*, 2023, pp. 1–5.
- [15] Z. Li, X. Chen, C.-M. Pun, and X. Cun, "High-resolution document shadow removal via a large-scale real-world dataset and a frequency-aware shadow erasing net," in *ICCV*, 2023, pp. 12 449–12 458.
- [16] S. Luo, X. Chen, W. Chen, Z. Li, S. Wang, and C.-M. Pun, "Devignet: High-resolution vignetting removal via a dual aggregated fusion transformer with adaptive channel expansion," in *AAAI*, 2024.
- [17] Z. Li, X. Chen, S. Wang, and C.-M. Pun, "A large-scale film style dataset for learning multi-frequency driven film enhancement," in *IJCAI*, 2023, pp. 1160–1168.
- [18] X. Guo, X. Chen, S. Luo, S. Wang, and C.-M. Pun, "Dual-hybrid attention network for specular highlight removal," in *ACM MM*, 2024.
- [19] Z. Li, X. Chen, S. Guo, S. Wang, and C.-M. Pun, "Wavenhancer: Unifying wavelet and transformer for image enhancement," *Journal of Computer Science and Technology*, vol. 39, no. 2, pp. 336–345, 2024.
- [20] R. Shen, X. Zhang, and Y. Xiang, "Affnet: attention mechanism network based on fusion feature for image cloud removal," *International Journal of Pattern Recognition and Artificial Intelligence*, vol. 36, no. 08, p. 2254014, 2022.
- [21] H. Li and C.-M. Pun, "Monocular robust 3d human localization by global and body-parts depth awareness," *IEEE Transactions on Circuits and Systems for Video Technology*, vol. 32, no. 11, pp. 7692–7705, 2022.
- [22] —, "Cee-net: complementary end-to-end network for 3d human pose generation and estimation," in *AAAI*, vol. 37, no. 1, 2023, pp. 1305–1313.
- [23] F. I. Diakogiannis, F. Waldner, P. Caccetta, and C. Wu, "Resunet-a: A deep learning framework for semantic segmentation of remotely sensed data," *ISPRS Journal of Photogrammetry and Remote Sensing*, vol. 162, pp. 94–114, 2020.
- [24] O. Ronneberger, P. Fischer, and T. Brox, "U-net: Convolutional networks for biomedical image segmentation," in *MICCAI*, 2015, pp. 234–241.
- [25] K. He, X. Zhang, S. Ren, and J. Sun, "Deep residual learning for image recognition," in *CVPR*, 2016, pp. 770–778.
- [26] A. Dosovitskiy, L. Beyer, A. Kolesnikov, D. Weissenborn, X. Zhai, T. Unterthiner, M. Dehghani, M. Minderer, G. Heigold, S. Gelly, J. Uszkoreit, and N. Houlsby, "An image is worth 16x16 words: Transformers for image recognition at scale," in *ICLR*, 2021.
- [27] Z. Liu, Y. Lin, Y. Cao, H. Hu, Y. Wei, Z. Zhang, S. Lin, and B. Guo, "Swin transformer: Hierarchical vision transformer using shifted windows," in *ICCV*, 2021, pp. 9992–10 002.
- [28] Q. Zhang and Y.-B. Yang, "Rest v2: simpler, faster and stronger," *NeurIPS*, vol. 35, pp. 36 440–36 452, 2022.
- [29] J. Chen, Y. Lu, Q. Yu, X. Luo, E. Adeli, Y. Wang, L. Lu, A. L. Yuille, and Y. Zhou, "Transunet: Transformers make strong encoders for medical image segmentation," *ArXiv*, 2021.
- [30] D. Jha, P. H. Smedsrud, D. Johansen, T. de Lange, H. D. Johansen, P. Halvorsen, and M. A. Riegler, "A comprehensive study on colorectal polyp segmentation with resunet++, conditional random field and test-time augmentation," *IEEE journal of biomedical and health informatics*, vol. 25, no. 6, pp. 2029–2040, 2021.
- [31] Z. Wang, X. Cun, J. Bao, W. Zhou, J. Liu, and H. Li, "Uformer: A general u-shaped transformer for image restoration," in *CVPR*, 2022, pp. 17 683–17 693.
- [32] X. Zhang, Y. Zhao, C. Gu, C. Lu, and S. Zhu, "Spa-former: An effective and lightweight transformer for image shadow removal," in *IJCNN*, 2023, pp. 1–8.
- [33] H. Wu, B. Xiao, N. Codella, M. Liu, X. Dai, L. Yuan, and L. Zhang, "Cvt: Introducing convolutions to vision transformers," in *ICCV*, 2021, pp. 22–31.
- [34] T. Huang, S. Li, X. Jia, H. Lu, and J. Liu, "Neighbor2neighbor: Self-supervised denoising from single noisy images," in *CVPR*, 2021, pp. 14 781–14 790.
- [35] Y. Li, K. Zhang, J. Cao, R. Timofte, and L. Van Gool, "Localvit: Bringing locality to vision transformers," *arXiv*, 2021.
- [36] M. Sandler, A. Howard, M. Zhu, A. Zhmoginov, and L.-C. Chen, "Mobilenetv2: Inverted residuals and linear bottlenecks," in *CVPR*, 2018, pp. 4510–4520.
- [37] K. Yuan, S. Guo, Z. Liu, A. Zhou, F. Yu, and W. Wu, "Incorporating convolution designs into visual transformers," in *ICCV*, 2021, pp. 579–588.
- [38] D. Hendrycks and K. Gimpel, "Gaussian error linear units (gelus)," *arXiv*, 2016.
- [39] F. Milletari, N. Navab, and S.-A. Ahmadi, "V-net: Fully convolutional neural networks for volumetric medical image segmentation," in *3DV*, 2016, pp. 565–571.
- [40] H. Cao, Y. Wang, J. Chen, D. Jiang, X. Zhang, Q. Tian, and M. Wang, "Swin-unet: Unet-like pure transformer for medical image segmentation," in *ECCV*, 2022, pp. 205–218.
- [41] Y. Tang, D. Yang, W. Li, H. R. Roth, B. Landman, D. Xu, V. Nath, and A. Hatamizadeh, "Self-supervised pre-training of swin transformers for 3d medical image analysis," in *CVPR*, 2022, pp. 20 730–20 740.
- [42] A. Hatamizadeh, Y. Tang, V. Nath, D. Yang, A. Myronenko, B. Landman, H. R. Roth, and D. Xu, "Unetr: Transformers for 3d medical image segmentation," in *WACV*, 2022, pp. 574–584.
- [43] H.-Y. Zhou, J. Guo, Y. Zhang, X. Han, L. Yu, L. Wang, and Y. Yu, "nn-former: volumetric medical image segmentation via a 3d transformer," *IEEE transactions on image processing*, 2023.
- [44] P. Bilic, P. Christ, H. B. Li, E. Vorontsov, A. Ben-Cohen, G. Kaissis, A. Szeskin, C. Jacobs, G. E. H. Mamani, G. Chartrand *et al.*, "The liver tumor segmentation benchmark (lits)," *Medical Image Analysis*, vol. 84, p. 102680, 2023.
- [45] *Proceedings of the Third International Symposium on Image Computing and Digital Medicine, ISICDM 2019, Xi'an, China, August 24-26, 2019*, 2019.
- [46] B. Landman, Z. Xu, J. Igelsias, M. Styner, T. Langerak, and A. Klein, "Miccai multi-atlas labeling beyond the cranial vault—workshop and challenge," in *MICCAI*, vol. 5, 2015, p. 12.
- [47] A. Dosovitskiy, L. Beyer, A. Kolesnikov, D. Weissenborn, X. Zhai, T. Unterthiner, M. Dehghani, M. Minderer, G. Heigold, S. Gelly *et al.*, "An image is worth 16x16 words: Transformers for image recognition at scale," in *ICLR*, 2020.
- [48] Y. Xie, J. Zhang, C. Shen, and Y. Xia, "Cotr: Efficiently bridging cnn and transformer for 3d medical image segmentation," in *MICCAI*, 2021, pp. 171–180.